

Supporting Information

One-pot Construction of Nitrogen-rich Polymeric Ionic Porous Networks for Effective CO₂ capture and fixation

Chenxiang Ai^a, Xinquan Ke^a, Juntao Tang^a, Xincun Tang^a, Raed Abu-Reziq^b, Jian Chang^c, Jinyin Yuan^{c,}, Guipeng Yu^{a,*}, Chunyue Pan^{a,*}*

^a *College of Chemistry and Chemical Engineering, Central South University, Changsha 410083, China*

^b *Institute of Chemistry, Casali Center of Applied Chemistry, The Center for Nanoscience and Nanotechnology, The Hebrew University of Jerusalem, Jerusalem 91904, Israel*

^c *Department of Materials and Environmental Chemistry, Stockholm University, Stockholm 10691, Sweden*

CONTENTS

Section S1. Materials

Section S2. Instruments and methods

Section S3. AEC measurements of model products and IPNs

Section S4. Determination for isosteric heat of adsorption

Section S5. Figures and Tables

Scheme S1 Synthetic route of Model C1

Scheme S2 Synthetic route of Model C2 and Model C3

Figure S1 ^1H NMR spectrum for Model C1

Figure S2 ^{13}C NMR spectrum for Model C1

Figure S3 Photography of ionic porous polymers IPN-CSU23

Figure S4 Possible routeline of IPN-CSUs

Table S1 Elemental analysis (EA) for IPN-CSU22 and IPN-CSU23

Figure S5 Thermo-gravimetric traces (TGA) for IPN-CSU2 and IPN-CSU23

Figure S6 PXRD patterns of IPN-CSU22 and IPN-CSU23

Figure S7 Scanning electron micrographs for IPN-CSU22(a, b) and IPN-CSU23(c,d)

Figure S8 TEM for IPN-CSU22 with different magnification

Figure S9 CO_2 adsorption/desorption curves of IPN-CSUs at 298K

Figure S10 Possible reaction mechanism for CO_2 conversion by IPN-CSUs

Table S2 CO_2 capacity and catalytic performance for model products

Figure S11 NMR analysis for crude products from catalytic experiments

Section S1. Materials

Cyanuric chloride, and 1*H*-imidazole were purchased from Alfa Aesar Chemical Inc. and used as received without further purification. 1-Methyl-2-pyrrolidinone, dichloromethane, acetone, tetrahydrofuran and chloroform were purified by distillation after removal of water over CaH₂ and stored with 4 Å molecular sieves prior to use. Unless otherwise stated, all other solvents or reagents used were commercially available and used without further purification.

Section S2. Instruments and methods

Using selected solvent mediums, hydrogen nuclear magnetic resonance (¹H NMR) and carbon nuclear magnetic resonance (¹³C NMR) spectroscopic measurements of the soluble samples were recorded on a Bruker AV-400 spectrometer with tetramethylsilane (TMS) as the internal reference. Solid-state ¹³C cross polarization magic angle spinning (¹³C CP/MAS) NMR spectra were obtained on a Bruker Avance III 400 NMR spectrometer. The spectra were obtained by using a contact time of 2.0 ms and a relaxation delay of 10.0 s. Using KBr disks, Fourier transform infrared spectroscopy (FT-IR) spectra of the powdered samples was collected in a transmission mode on a VARIAN 1000 FT-IR (scimitar series) spectrometer. Elemental analysis including carbon, hydrogen, and nitrogen was collected on a FlashEA 2000 Elemental Analyzer using a CHN model. Scanning electron microscopy (SEM) and Energy Dispersive X-ray spectroscopy (EDS) experiments were performed on a FEI Quanta-200 scanning electron microscope. For Transmission electron microscopy (TEM) measurements, samples were coated with a thin film of platinum. It was carried out on a JEOL JEM 3010 at 300 kV. Powder X-ray Diffraction (PXRD) pattern of the samples

was collected on a Bruker AXS D8 Discover multi-purpose high power X-ray diffractometer. Thermogravimetric analysis (TGA) was performed using a PERKIN ELMER TGA7 instrument, and the samples was investigated from 25 °C to 800 °C at a heating rate of 10 K min⁻¹ under N₂ atmosphere. The nitrogen adsorption and desorption isotherms were obtained by using ASAP 2020 volumetric adsorption analyzer at 77 K, and the surface area and pore size distribution of the sample were obtained using Bruner-Emmett-Teller (BET) and Barrett-Joyner-Halenda (BJH) models. The sample was degassed at 80 °C for 9 h under vacuum (5×10^{-4} Pa) before the analysis. The cumulative apparent surface area for N₂ was calculated by using the BET model range from 0.025 to 0.10 bar for the sample. The pore size distribution of sample was calculated from the adsorption branches of the isotherms according to the Nonlocal Density Functional Theory (NLDFT) method by using a carbon slit pore model. The low-pressure nitrogen adsorption and desorption isotherms were measured at 273K. The adsorption and desorption isotherms of carbon dioxide (CO₂) were obtained from the ASAP 2020 volumetric adsorption analyzer at 273 K and 298 K up to 1 bar. Isosteric heat of adsorption (Q_{ST}) value of the samples towards nitrogen or CO₂ was calculated by using Clausius-Clapeyron equation on the data master offline data reduction software (Micrometrics). For the catalytic cycloaddition of CO₂ and epoxides, the reaction mixture after centrifugation to remove the IPN-CSUs catalyst was analysed by ¹H NMR spectroscopy to calculate the reaction yield.

Section S3. AEC measurements of model products and IPNs

The anion exchange capacity (AEC, chloride form) of model reaction products:

Model C1 (0.3 g) were dissolved in concentrated nitric acid and then 0.1M silver nitrate solution in water was added dropwise to the clear solution. Finally, silver chloride as precipitate was isolated and washed by acetone, and dried under vacuum till constant weight. Yield: 0.15 g, corresponding to an AEC value of 3.4 mmol g⁻¹.

AEC of IPF-CSUs: Typically, IPF-CSU-22 (0.3 g) was dissolved in concentrated nitric acid and the undissolved substance was filtered off to obtain a clear mixture solution. Secondly, 0.1M aqueous silver nitrate solution was added dropwise to the clear mixture solution in the condition of potassium chromate as indicator. Then, silver chloride as precipitate was isolated and washed by acetone, and finally dried under vacuum till constant weight.

Section S4. Determination for isosteric heat of adsorption

The adsorption enthalpies of these porous materials on CO₂ molecules were calculated by the adsorption isotherms at different temperatures (such as 273K and 298K) to study the binding ability of IPN-CSU adsorbent molecules to small gas molecules. It is clear that physical adsorption and chemical adsorption can be defined by the size of adsorption enthalpy. Combining the CO₂ adsorption isotherms at 273K and 298K, the Clausius–Clapeyron equation is fitted to calculate the adsorption enthalpy. The equation is as follows:

$$Q_{st} = R \times T_1 \times T_2 (\ln P_1/P_2)/(T_1 - T_2) \quad (1)$$

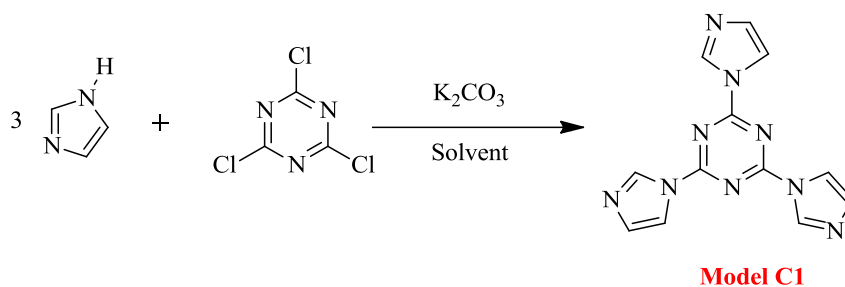
Q_{st} is the adsorption enthalpy of CO₂ by the porous body, R is the gas constant, and P_1 and P_2 are the corresponding CO₂ adsorption capacity at $T_1=273K$ and $T_2=298K$ respectively.

Section S4. Catalytic conversion of CO₂ to cyclic carbonates

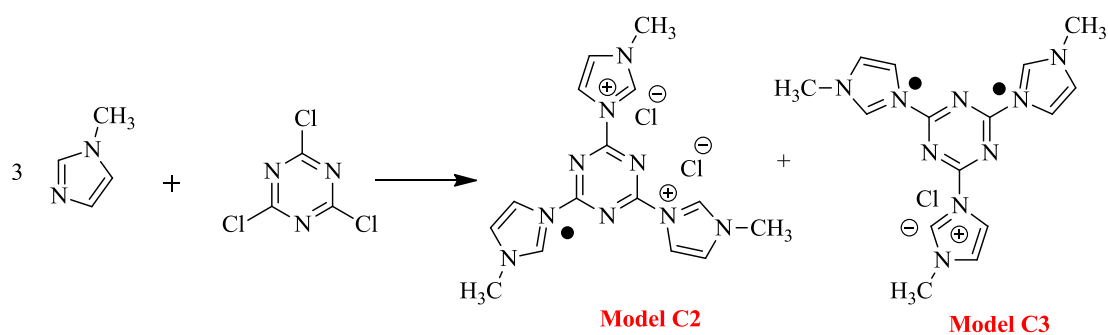
Catalytic procedures: A 3-neck round bottom flask was charged with IPN-CSUs catalyst (0.098 mmol), the epoxide 2-methyloxirane (12.5 mmol) with or without TBAB catalyst (1.44 mmol). Then, CO₂ (0.1 Mpa) was poured into the reactor as a reactant. The reaction mixture was stirred at 25 °C for 48 h, after which the remaining

CO₂ was slowly evaporated. After centrifugation to remove the catalyst, the reaction mixture was analyzed by ¹H NMR spectroscopy to determine the reaction yield.

Section S4 Figures and tables



Scheme S1 Synthetic route of Model C1.



Scheme S2 Synthetic route of Model C2 and Model C3.

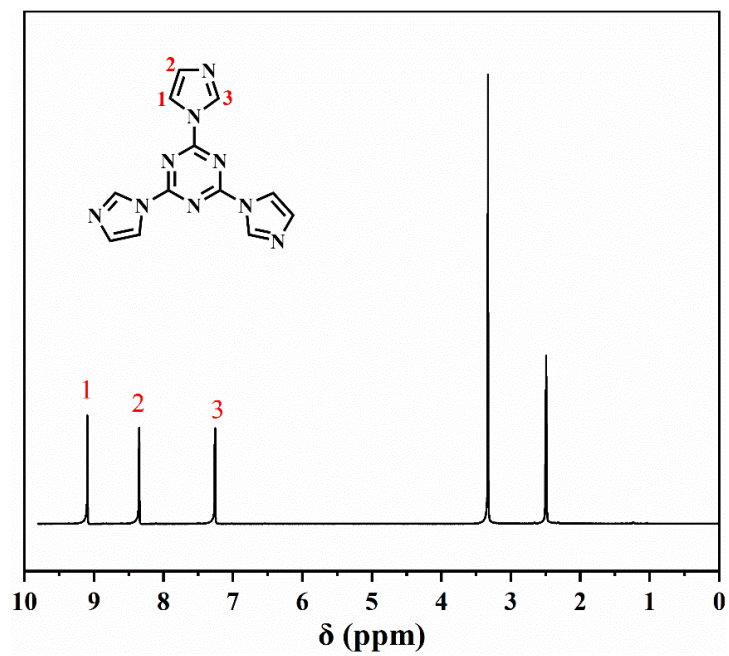


Figure S1 ¹H NMR spectrum for Model C1.

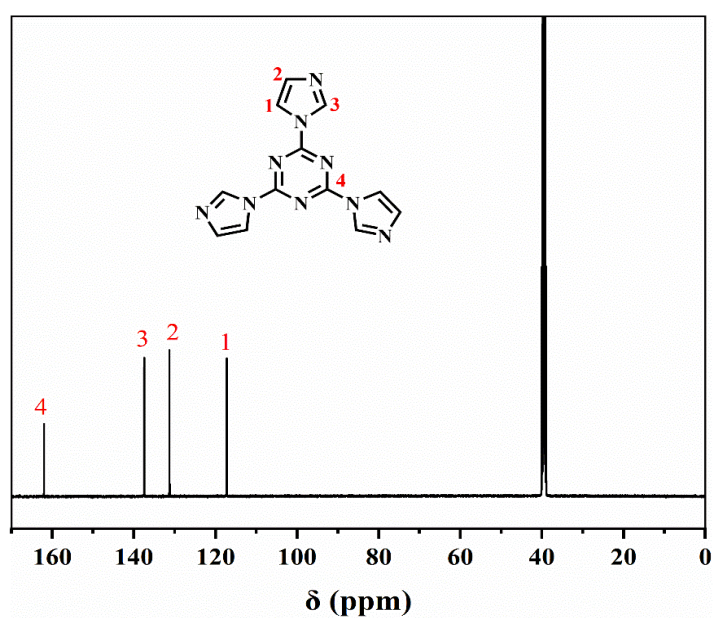


Figure S2 ¹³C NMR spectrum for Model C1.

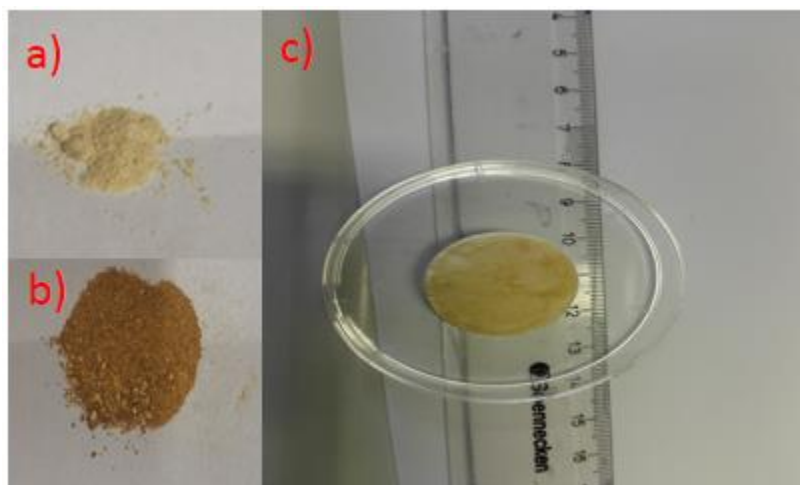


Figure S3 Photography of ionic porous polymers IPN-CSU23.

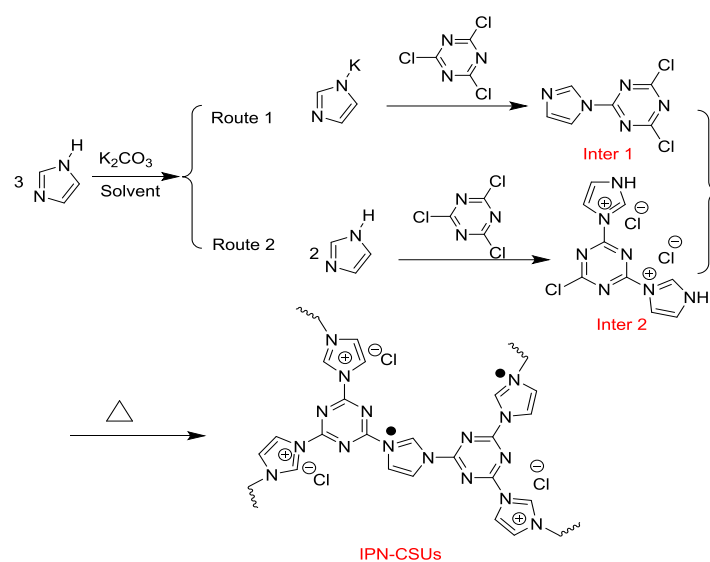


Figure S4 Possible routine of IPN-CSUs.

Table S1 Elemental analysis (EA) for IPN-CSU22 and IPN-CSU23.

Sample	EA theoretical value			EA found		
	C	N	H	C	N	H
IPN-CSU22	32.41	33.59	2.42	33.42	33.37	2.28
IPN-CSU23	32.41	33.59	2.42	33.08	33.01	2.09

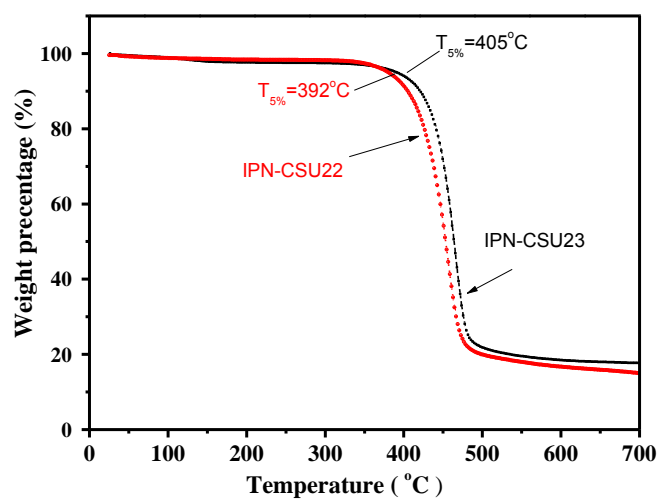


Figure S5 Thermo-gravimetric traces (TGA) for IPN-CSU2 and IPN-CSU23.

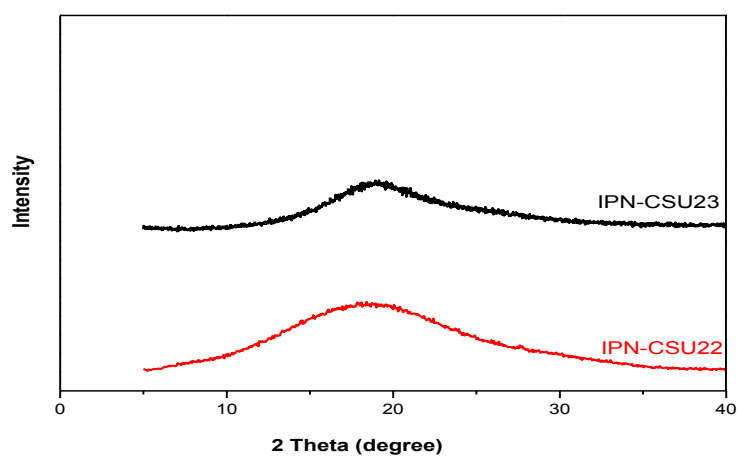


Figure S6 PXRD patterns of IPN-CSU22 and IPN-CSU23.

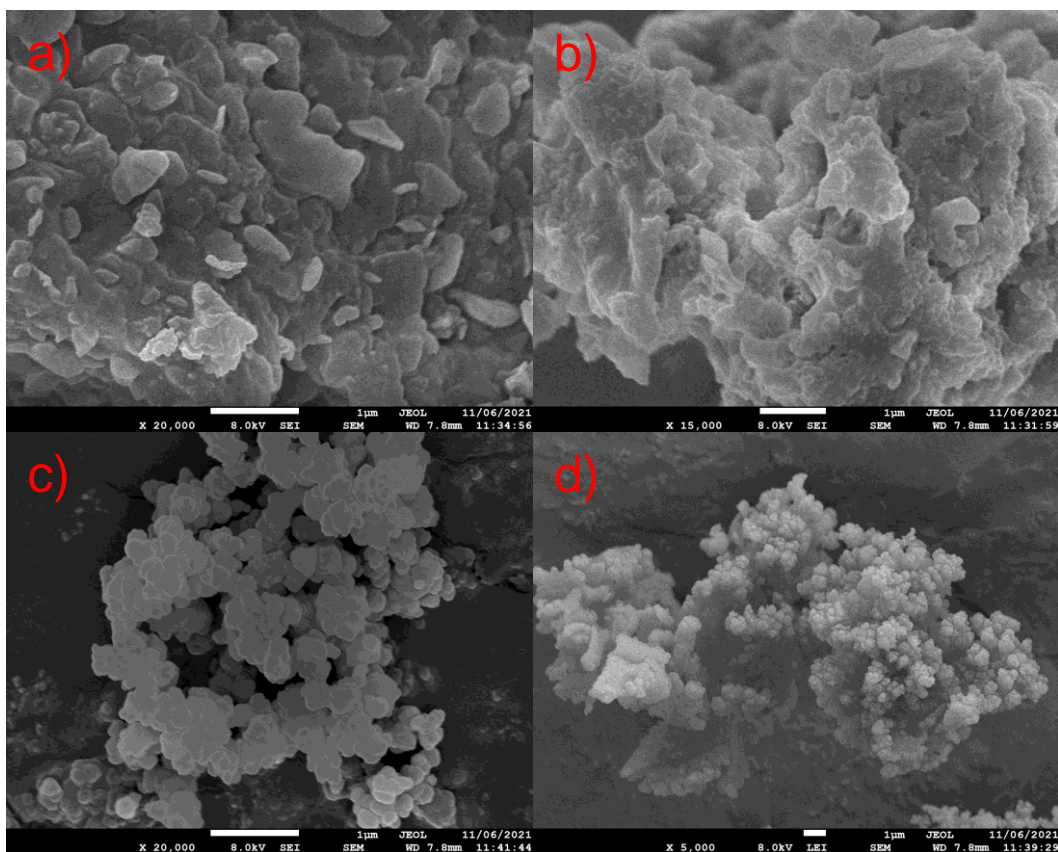


Figure S7 SEM images for IPN-CSU22(a, b) and IPN-CSU23(c,d).

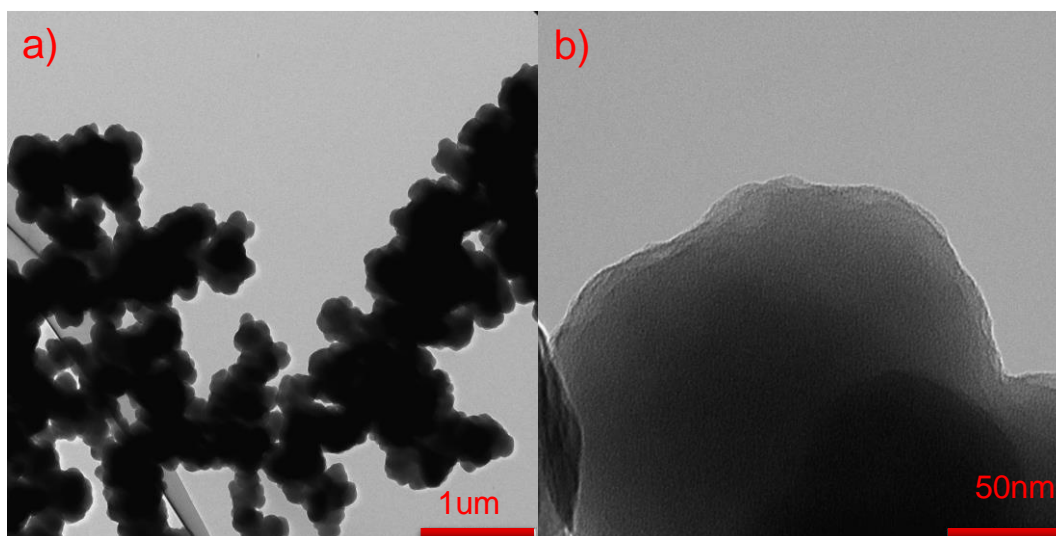


Figure S8 TEM images for IPN-CSU22 with different magnification.

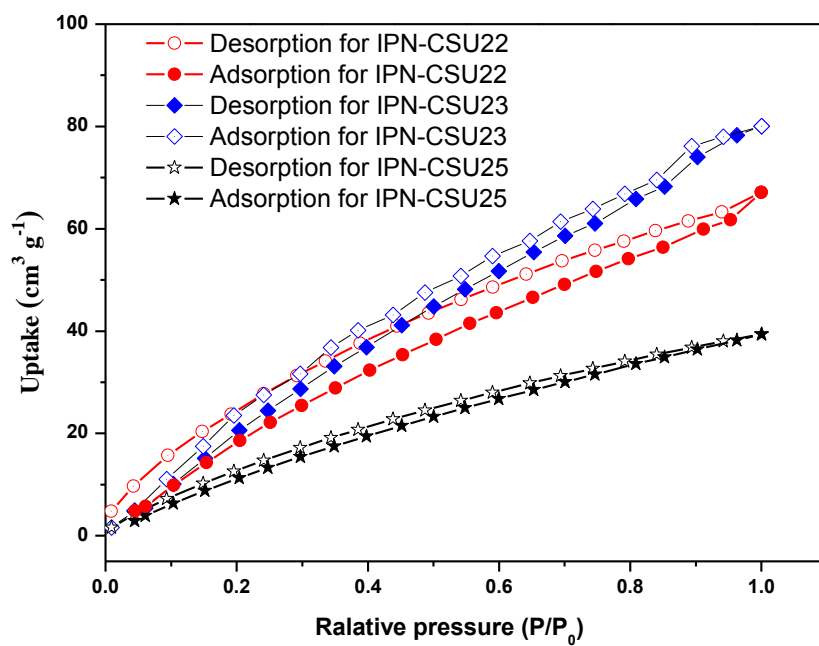


Figure S9 CO₂ adsorption/desorption curves of IPN-CSUs at 273K.

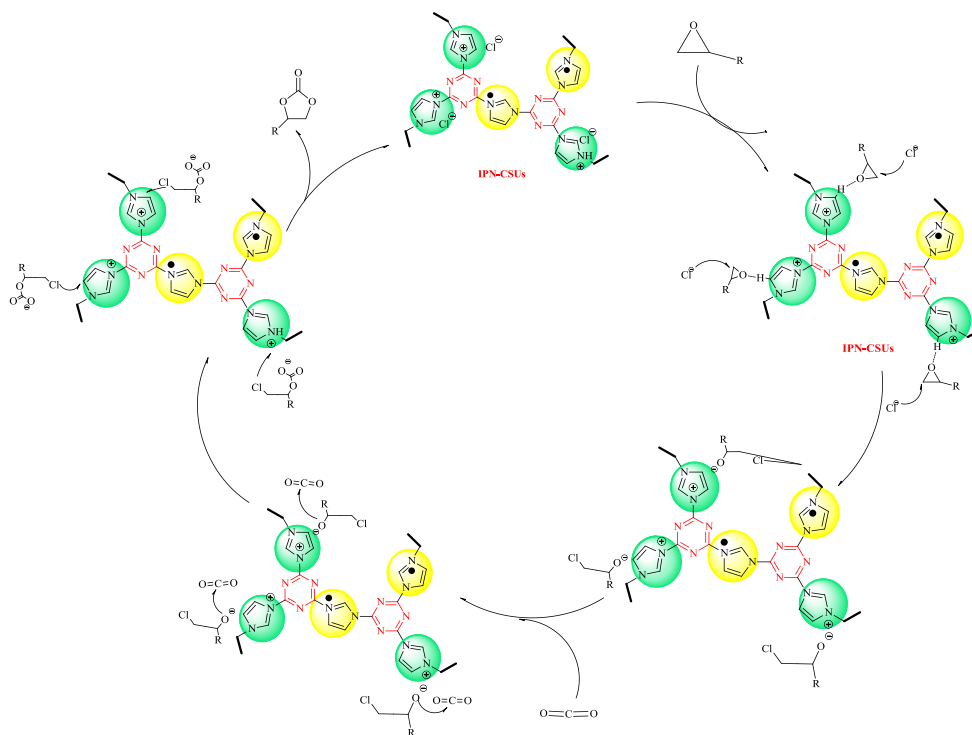


Figure S10 Possible reaction mechanism for CO₂ conversion by IPN-CSUs.

Table S2 CO₂ capacity and catalytic performance for model products

Sample	CO ₂ capacity		Catalytic fixation			
	CO ₂ adsorption capacity ^a (cc/g)	Selectivity (v/v) ^b	Time (h)	Pressure (MPa)	Temp. (°C)	Yield ^c (%)
Model C1	2.1	3.9	33.42	33.37	2.28	- ^d
Model C2/C3	11.4	9.8	33.08	33.01	2.09	11.6

^a 273 K and 1 bar. ^b Selectivity: initial ideal selectivity; ^c The yield of 4-methyl-1,3-dioxolan-2-one over

model compound catalysts without the presence of TBAB (Determined by ¹HNMR). ^d Not detected

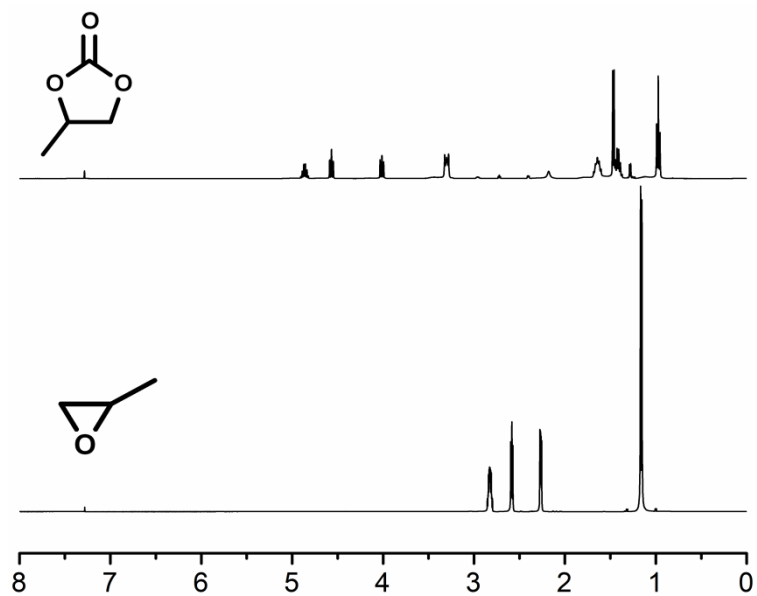


Figure S11 ¹H NMR (400 MHz, CDCl₃, 298 K) spectra of propylene oxide and its corresponding cyclic carbonate (crude sample) over IPN-CSUs/TBAB at 298K for 48 h.